SciencePG
Science Publishing Group

Evaluation of the Impact of Biofield Energy Healing Treatment (The Trivedi Effect®) on the Physicochemical, Thermal, Structural, and Behavioral Properties of Magnesium Gluconate

Mahendra Kumar Trivedi[1], Alice Branton[1], Dahryn Trivedi[1], Gopal Nayak[1], Aileen Carol Lee[1], Aksana Hancharuk[1], Carola Marina Sand[1], Debra Jane Schnitzer[1], Rudina Thanasi[1], Eileen Mary Meagher[1], Faith Ann Pyka[1], Gary Richard Gerber[1], Johanna Catharina Stromsnas[1], Judith Marian Shapiro[1], Laura Nelson Streicher[1], Lorraine Marie Hachfeld[1], Matthew Charles Hornung[1], Patricia M. Rowe[1], Sally Jean Henderson[1], Sheila Maureen Benson[1], Shirley Theresa Holmlund[1], Stephen P. Salters[1], Parthasarathi Panda[2], Snehasis Jana[2, *]

[1]Trivedi Global, Inc., Henderson, Nevada, USA

[2]Trivedi Science Research Laboratory Pvt. Ltd., Bhopal, Madhya Pradesh, India

Email address:

publication@trivedieffect.com (S. Jana)

*Corresponding author

To cite this article:

Mahendra Kumar Trivedi, Alice Branton, Dahryn Trivedi, Gopal Nayak, Aileen Carol Lee, Aksana Hancharuk, Carola Marina Sand, Debra Jane Schnitzer, Rudina Thanasi, Eileen Mary Meagher, Faith Ann Pyka, Gary Richard Gerber, Johanna Catharina Stromsnas, Judith Marian Shapiro, Laura Nelson Streicher, Lorraine Marie Hachfeld, Matthew Charles Hornung, Patricia M. Rowe, Sally Jean Henderson, Sheila Maureen Benson, Shirley Theresa Holmlund, Stephen P. Salters, Parthasarathi Panda, Snehasis Jana. Evaluation of the Impact of Biofield Energy Healing Treatment (The Trivedi Effect®) on the Physicochemical, Thermal, Structural, and Behavioral Properties of Magnesium Gluconate. *International Journal of Nutrition and Food Sciences*. Vol. 6, No. 2, 2017, pp. 71-82. doi: 10.11648/j.ijnfs.20170602.13

Abstract: Magnesium gluconate is a classical organometallic salt used for the prevention and treatment of magnesium deficiency diseases. The objective of the current research was to explore the influence of The Trivedi Effect® - Energy of Consciousness Healing Treatment on the physicochemical, thermal and behavioral properties of magnesium gluconate using PXRD, PSD, FT-IR, UV-vis spectroscopy, TGA, and DSC analysis. Magnesium gluconate was divided into two parts – one part was control without any Biofield Energy Treatment, while another part was treated with the Biofield Energy Healing Treatment remotely by eighteen renowned Biofield Energy Healers and defined as the Biofield Energy Treated sample. The PXRD analysis exhibited significant alteration of the crystal morphology of the treated sample compared with the control sample. The crystallite size of the treated sample was remarkably changed from range -33.33% to 66.65% compared with the control sample. The average crystallite size was increased in the treated sample by 6.13% compared with the control sample. Particle size analysis revealed that the particle size at d_{10} value was significantly reduced in the treated sample by 13.20% compared with the control sample, although the particle size at d_{50} and d_{90} values were increased in the treated sample by 2.75% and 3.72%, respectively. The treated sample's surface area was significantly enhanced (6.96%) compared with the control sample. The FT-IR and UV-vis analysis showed that the structure of magnesium gluconate remained similar in both the treated and control samples. The TGA analysis revealed that the weight loss of the first and second degradation steps in the treated sample was significantly decreased by 2.89% and 8.43%, respectively compared with the control sample, whereas at the third degradation step, the weight loss was enhanced by 14.80% compared with the control sample. The DSC analysis revealed that the melting point of the control and treated samples were 170.23°C and 170.25°C, respectively. The latent heat of fusion was significantly decreased by 6.15% in the treated sample compared with the control sample. The current study infers that The Trivedi Effect® - Energy of Consciousness Healing Treatment might lead to a new polymorphic form of magnesium gluconate, which could be more soluble and bioavailable compared with the untreated compound. Hence, the Biofield Energy

Treated magnesium gluconate would be very useful to design better nutraceutical and/or pharmaceutical formulations that might offer better therapeutic responses against inflammatory diseases, immunological disorders, stress, aging and other chronic infections.

1. Introduction

Magnesium ion (Mg^{2+}) is a major intracellular ion and plays an important role in the regulation of tRNA and rRNA structures. This ion is also a crucial cofactor for many RNA and DNA processing enzymes as well as for those enzymes using AMP, ADP, or ATP as substrates [1-3]. Hence, magnesium ion is an essential mineral element in human and animal nutrition. It is also used as a metallotherapeutic agent to treat various diseases such as asthma, arrhythmias, acute myocardial infarction, gestational hypertension, preeclampsia and eclampsia [1-8]. Perioperative magnesium supplementation is found to be very useful in the management of postoperative pain by inhibiting postoperative hypomagnesia as well as reducing the incidence of postoperative shivering [9, 10]. Gluconic acid is a minor organic acid formed from glucose through a simple dehydrogenation reaction catalyzed by glucose oxidase. Gluconic acid and its derivatives are commonly used in the food and pharmaceutical industry [11]. Magnesium gluconate ($MgC_{12}H_{22}O_{14}$) is the magnesium salt of gluconic acid. It is used by itself or in combination with one or more antioxidants for the prevention and treatment of diabetes mellitus, allergies, septic shock, inflammatory diseases, immunological disorders, and other chronic infections [12, 13]. It can be used intravenously in the treatment of ischemia/reperfusion injury due to oxidative stress in order to block free radical flow [14]. This salt is used as an oral tocolytic agent in women, whose labor is arrested initially with intravenous therapy by acting on non-selective β-receptor [15]. The scientific literature reports that magnesium gluconate is a more powerful antioxidant than other magnesium salts [12]. Moreover, magnesium gluconate is a physiologically acceptable salt among from the other salt forms [13]. The literature data mentions that the bioavailability of magnesium is less in humans because they have difficulties in absorption through the narrow channels in their biological membranes due to the higher steric constraints for magnesium transporters and incapability of its hydration shell [16, 17]. Magnesium gluconate, which shows the most magnesium absorption and retention values, displayed the highest bioavailability among the magnesium salts such as chloride, sulfate, carbonate, acetate, citrate, lactate, aspartate, etc. [18]. In this point of view, a novel proprietary herbomineral formulation was designed as a nutraceutical supplement, and can be used for the prevention and treatment of various human disorders. Magnesium gluconate is one of the components

in this novel proprietary herbomineral formulation as the source of magnesium.

Since ancient times, many different cultures, religions and systems of belief have recognized a living force that preserves and inhabits every living organism. This force is the source of 'life' and has been called various names, such as prana by the Hindus, *qi* or *chi* by the Chinese, and *ki* by the Japanese. This is believed to co-relate with the soul, spirit and mind. This hypothetical vital force has been scientifically evaluated and is now considered the Bioenergetics Field. The Biofield Energy is a dynamic electromagnetic field surrounding the human body, resulting from the continuous emission of low-level light, heat, and acoustical energy from the body. Biofield Energy is infinite, paradimensional and can freely flow between the human and environment [19, 20]. So, a human has the ability to harness energy from the ionosphere of the earth, the "universal energy field", and transmit it to any living organism (s) or nonliving object (s) around the globe. The object or recipient always receives the energy and responds in a useful way. This process is known as The Trivedi Effect® - Energy of Consciousness Healing Treatment [21]. Biofield (Putative Energy Field) based Energy Therapies are used worldwide to promote health and healing. The National Center of Complementary and Integrative Health (NCCIH) has recognized and accepted Biofield Energy Healing as a Complementary and Alternative Medicine (CAM) health care approach in addition to other therapies, medicines and practices such as natural products, deep breathing, yoga, Tai Chi, Qi Gong, chiropractic/osteopathic manipulation, meditation, massage, special diets, homeopathy, progressive relaxation, guided imagery, acupressure, acupuncture, relaxation techniques, hypnotherapy, healing touch, movement therapy, pilates, rolfing structural integration, mindfulness, Ayurvedic medicine, traditional Chinese herbs and medicines, naturopathy, essential oils, aromatherapy, Reiki, cranial sacral therapy and applied prayer (as is common in all religions, like Christianity, Hinduism, Buddhism and Judaism) [22]. Biofield Energy Healing Treatment (The Trivedi Effect®) has been published in numerous peer-reviewed science journals due to its significant impacts in the science fields of biotechnology, genetics, cancer, microbiology, materials science, agriculture, and pharmaceuticals. These publications reported that Biofield Energy Treatment (The Trivedi Effect®) has the

astounding capability to transform the physical, structural, chemical, thermal and behavioral properties of several pharmaceuticals [23-25], nutraceuticals [26, 27], organic compounds [28-30], metals and ceramics in materials science [31-33], improve the overall productivity of crops [34-36], as well as modulate the efficacy of various living cells [37-40]. Although magnesium gluconate exhibits the highest bioavailability and moderate solubility in water in comparison to other magnesium salts, humans still face problems in achieving their daily requirements of magnesium [41]. The physical and chemical properties such as particle size, crystalline structure, crystallite size, surface area, etc. of a pharmaceutical have a direct influence on the absorption, dissolution, and bioavailability of the drug [42]. The stability of a solid drug with respect to the atmospheric conditions is very important to the pharmaceutical industry during processing, formulation, storage, and packaging in order to achieve better therapeutic efficacy [43]. Biofield Energy Treatment (The Trivedi Effect®) has been reported to change the particle size, specific surface area, crystalline, chemical and thermal behavior of an atom/ion through possible mediation of neutrinos [44]. By considering these aspects, the physicochemical, structural, thermal and behavioral properties of the Biofield Energy Treated and untreated magnesium gluconate were studied through various analytical techniques including powder X-ray diffraction (PXRD), particle size distribution analysis (PSD), Fourier transform infrared (FT-IR) spectrometry, ultraviolet-visible (UV-vis) spectroscopy, thermogravimetric analysis (TGA), and differential scanning calorimetry (DSC).

2. Materials and Methods

2.1. Chemicals and Reagents

Magnesium gluconate hydrate was procured from Tokyo Chemical Industry Co., Ltd. (TCI), Japan. All the other chemicals used in this experiment were of analytical grade procured from local vendors.

2.2. Biofield Energy Treatment Strategies

Magnesium gluconate was one of the components of the new proprietary herbomineral formulation, which was developed by our research team and was used *per se* as the test compound for the current study. The test compound was divided into two parts, one part of the test compound was treated with the Biofield Energy by eighteen renowned Biofield Energy Healers (The Trivedi Effect®) and defined as the Biofield Energy Treated sample, while the second part of the test compound did not receive any sort of treatment and was defined as the untreated or control magnesium gluconate sample. The Biofield Energy Treatment was provided by the group of eighteen renowned Biofield Energy Healers (The Trivedi Effect®), who participated in this study and performed the Biofield

Energy Treatment remotely. Eleven Biofield Energy Healers were remotely located in the U. S. A., four remotely located in Canada, two remotely located in Finland, and one of which was remotely located in Albania, while the test compound was located in the research laboratory of GVK Biosciences Pvt. Ltd., Hyderabad, India. This Biofield Treatment was provided for 5 minutes through the Healer's Unique Energy Transmission process remotely to the test compound, which was kept under laboratory conditions. None of the Biofield Energy Healers in this study visited the laboratory in person, nor had any contact with the compounds. Similarly, the control compound was subjected to "sham" healer for 5 minutes, under the same laboratory conditions. The sham healer did not have any knowledge about the Biofield Energy Treatment. After that, the Biofield Energy Treated and untreated samples were kept in similar sealed conditions and characterized thoroughly by PXRD, PSD, FT-IR, UV-visible spectroscopy, TGA, and DSC analysis.

2.3. Characterization

2.3.1. Powder X-ray Diffraction (XRD) Analysis

The XRD analysis was performed on PANalytical X'pert Pro powder X-ray diffractometer system. The X-ray of wavelength 1.54056 Å was used. The data was collected in the form of a chart of the Bragg angle (2θ) *vs.* intensity, and a detailed table containing information on peak intensity counts, d value (Å), relative intensity (%), full width half maximum (FWHM) ($\theta°$). From the XRD results, the crystallite size (G) was calculated using X'pert data collector and X'pert high score plus processing software. The crystallite size (G) was calculated from the Scherrer equation [45, 46]. The method was based on the width of the diffraction patterns obtained in the X-ray reflected crystalline region. The crystallite size (G) was calculated by using the following equation 1:

$$G = k\lambda / (bCos\theta) \qquad (1)$$

Where, k is the equipment constant (0.5), λ is the X-ray wavelength (0.154 nm); b in radians is the full-width at half of the peaks and θ is the corresponding Bragg angle.

Percent change in crystallite size (G) was calculated using the following equation 2:

$$\% \text{ change in crystallite size} = \frac{[G_{Treated} - G_{Control}]}{G_{Control}} \times 100 \qquad (2)$$

Where, $G_{Control}$ and $G_{Treated}$ are the crystallite size of the control and Biofield Energy Treated samples, respectively.

A total of 500.18 mg of the control and Biofield Energy Treated samples individually were used for the analysis and prepared by the back loading technique using the sample preparation kit. The sample was spread on the holder ring in sufficient quantity to fill the ring cavity. It was then pressed down using a powder press block and scrapped the powder that was in surplus using a glass slide in order to get a densely packed specimen. The bottom

plate was placed onto the holder ring and clamped in position. The sample holder was then removed from the sample preparation table by turning it upside down. A smooth surface of the sample was obtained to ensure optimum results.

2.3.2. Particle Size Distribution (PSD) Analysis

The average particle size and particle size distribution were analyzed using Malvern Mastersizer 2000, UK, with a detection range from 0.01 μm to 3000 μm. The sample unit was filled with dispersant medium and operated the stirrer at 2500 rpm. Alignment of the optics was done and taken the background measurement. After the background measurement, the sample was added in to the sample unit with constant monitoring of the obscuration. When the obscuration of the sample reached in between 15% and 20%, further addition of the sample stopped. When the obscuration was stable, the measurement was taken twice and the average was taken of the two measurements. The average histogram of the two measurements was recorded. Along with the histogram, the data are presented in a table format, which include particle size (μm). Also, the values for particle size (μm) for at below 10% level (d_{10}), 50% level (d_{50}), and 90% level (d_{90}) were calculated from the histogram and the calculations were done using Mastersizer 2000 software.

The percent change in particle size (d) for at below 10% level (d_{10}), 50% level (d_{50}), and 90% level (d_{90}) was calculated using the following equation 3:

$$\% \text{ change in particle size} = \frac{[d_{Treated} - d_{Control}]}{d_{Control}} \times 100 \quad (3)$$

Where, $d_{Control}$ and $d_{Treated}$ are the particle size (μm) for at below 10% level (d_{10}), 50% level (d_{50}), and 90% level (d_{90}) of the control and Biofield Energy Treated samples, respectively.

The percent change in surface area (S) was calculated using the following equation 4:

$$\% \text{ change in surface area} = \frac{[S_{Treated} - S_{Control}]}{S_{Control}} \times 100 \quad (4)$$

Where, $S_{Control}$ and $S_{Treated}$ are the surface area of the control and Biofield Energy Treated samples, respectively.

2.3.3. Fourier Transform Infrared (FT-IR) Spectroscopy

FT-IR spectroscopy of magnesium gluconate was performed using Spectrum Two (Perkin Elmer, USA) Fourier Transform Infrared Spectrometer with the frequency range of 400-4000 cm^{-1} by using the pressed KBr disk technique.

2.3.4. Ultraviolet-Visible Spectroscopy (UV-Vis) Analysis

The UV-Vis spectral analysis was carried out using Shimadzu UV-2450 with UV Probe, Japan. The spectrum was recorded using 1 cm quartz cell with a slit width of 1.0 nm. The wavelength range chosen for recording the spectra was 190-800 nm. The absorbance spectra (in the range of 0.2 to 0.9) and absorbance maximum (λ_{max}) were

recorded.

2.3.5. Thermal Gravimetric Analysis (TGA)

The TGA analysis was performed using TGA Q50 (TA Instruments, USA) at a heating rate of 10°C/min from room temperature *i.e.* 25°C to 900°C in a nitrogen atmosphere. A total of 15 mg of sample was weighed in a platinum crucible. In TGA, the weight loss for each step was recorded in grams as well as in percent loss with respect to the initial weight. Also, the onset, endset, and peak temperature for each step were recorded in TGA. In DTG, the onset, endset, peak temperature and integral area of the peak and change in heat (J/g) of each peak were recorded.

Percent change in weight loss (W) was calculated using the following equation 5:

$$\% \text{ change in weight loss} = \frac{[W_{Treated} - W_{Control}]}{W_{Control}} \times 100 \quad (5)$$

Where, $W_{Control}$ and $W_{Treated}$ are the weight loss of the control and Biofield Energy Treated samples, respectively.

2.3.6. Differential Scanning Calorimetry (DSC)

Analysis was performed using the DSC Q20 (TA Instruments, USA) Differential Scanning Calorimeter. A total of 8.23 mg of sample was weighed and sealed in an aluminum pan and equilibrated at 25°C and heated up to 450°C at the heating rate of 10°C/min under nitrogen gas as purge atmosphere with the flow rate of 50 mL/min. The value for onset, endset, peak temperature, peak height (mJ or mW), peak area, and change in heat (J/g) for each peak were recorded.

The percent change in melting point (T) was calculated using the following equation 6:

$$\% \text{ change in melting point} = \frac{[T_{Treated} - T_{Control}]}{T_{Control}} \times 100 \quad (6)$$

Where, $T_{Control}$ and $T_{Treated}$ are the melting point of the control and Biofield Energy Treated samples, respectively.

The percent change in the latent heat of fusion (ΔH) was calculated using the following equation 7:

$$\% \text{ change in Latent heat of fusion} = \frac{[\Delta H_{Treated} - \Delta H_{Control}]}{\Delta H_{Control}} \times 100 \quad (7)$$

Where, $\Delta H_{Control}$ and $\Delta H_{Treated}$ are the latent heat of fusion of the control and Biofield Energy Treated samples, respectively.

3. Results and Discussion

3.1. Powder X-ray Diffraction (PXRD) Analysis

The PXRD diffractograms of both the control and Biofield Energy Treated samples (Figure 1), exhibited sharp and intense peaks indicating that both of the samples were crystalline in nature.
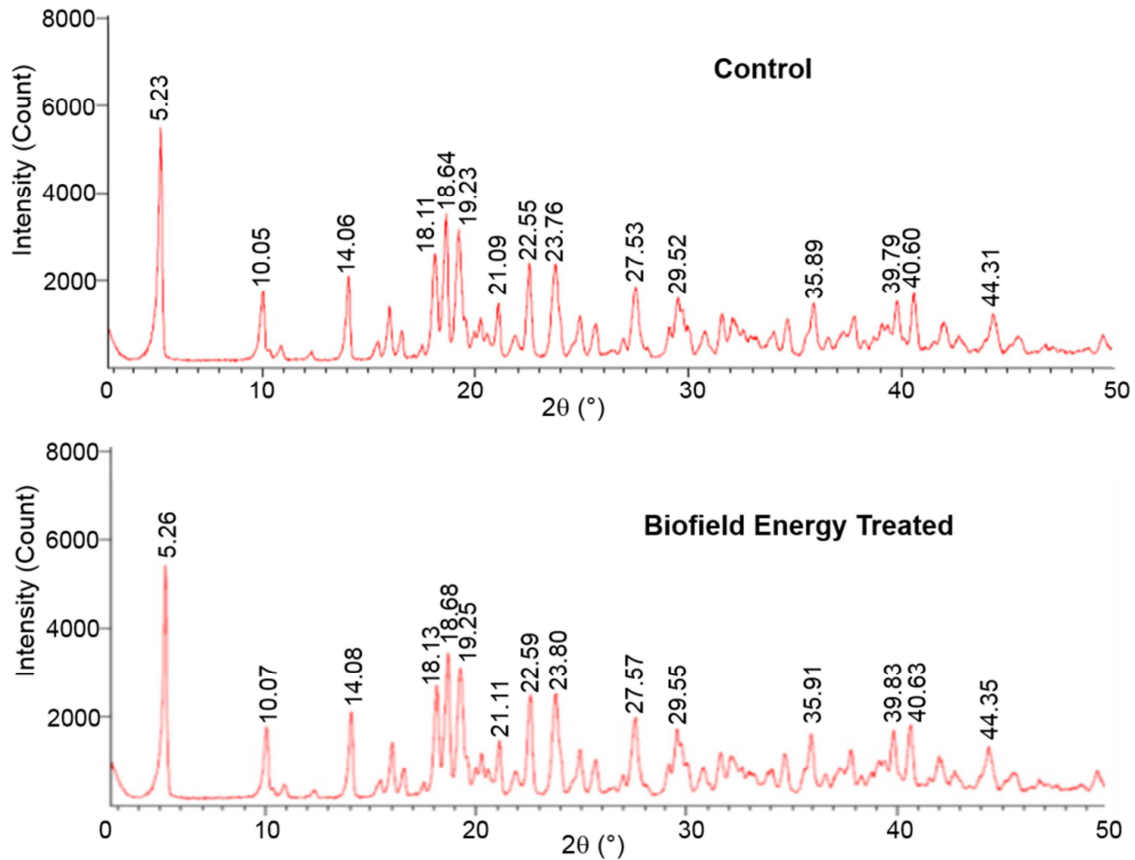
Figure 1. Powder X-ray diffractograms of the control and Biofield Energy Treated magnesium gluconate.

PXRD data such as the Bragg angle (2θ), relative intensity (%), full width half maximum (FWHM) (θ°), and crystallite size (G) for the control and Biofield Energy Treated samples are presented in Table 1. The crystallite size was calculated using Scherrer equation [45, 46].

Table 1. PXRD data for the control and Biofield Energy Treated magnesium gluconate.

Entry No.	Bragg angle (°2θ)		Relative Intensity (%)		FWHM (°2θ)		Crystallite size (G, nm)		
	Control	Treated	Control	Treated	Control	Treated	Control	Treated	% change[*]
1	5.23	5.26	100.00	100.00	0.1171	0.1506	37.63	29.26	-22.24
2	10.05	10.07	29.40	29.88	0.1840	0.1338	24.01	33.02	37.52
3	14.06	14.08	35.85	37.19	0.1506	0.1673	29.45	26.51	-9.98
4	18.11	18.13	45.42	48.71	0.1338	0.2007	33.31	22.21	-33.33
5	18.64	18.68	62.70	62.70	0.2342	0.1673	19.05	26.66	40.00
6	19.23	19.25	55.20	55.91	0.2007	0.1840	22.24	24.26	9.08
7	21.09	21.11	24.14	24.81	0.1673	0.1338	26.76	33.46	25.04
8	22.55	22.59	40.94	44.60	0.1506	0.2007	29.80	22.37	-24.96
9	23.76	23.80	40.94	44.08	0.2007	0.1673	22.41	26.89	19.97
10	27.53	27.57	30.99	34.78	0.1673	0.1004	27.09	45.15	66.65
11	29.52	29.55	26.46	29.57	0.1338	0.1673	34.02	27.21	-20.02
12	35.89	35.91	24.11	27.96	0.1673	0.1224	27.66	37.81	36.69
13	39.79	39.83	24.50	29.19	0.2175	0.1428	21.53	32.79	52.33
14	40.60	40.63	28.22	31.35	0.1673	0.2244	28.06	20.92	-25.44
15	Average crystallite size						27.75	29.45	6.13

FWHM: Full width half maximum, [*]denotes the percentage change in the crystallite size of the Biofield Energy Treated sample with respect to the control sample.

Table 1 displays the changes of the crystallite size and relative intensities along with other XRD peaks in the Biofield Energy Treated magnesium gluconate compared with the control sample. The crystallite size of the control and Biofield Energy Treated samples at the highest intense peak were 37.63 and 29.26 nm, respectively (Table 1, entry

1). This result showed that the crystallite size of the Biofield Energy Treated sample was reduced by 22.24% as compared to the control sample. In addition, the crystallite size values of the Biofield Energy Treated sample at 2θ equal to nearly 14.1°, 18.1°, 22.6°, 29.6°, and 40.6° (Table 1, entry 3, 4, 8, 11, and 14) were significantly decreased from 10% to 33% with respect to the control sample. Furthermore, at position 2θ equal to nearly 10.1°, 18.7°, 19.3°, 21.1°, 23.8°, 27.6°, 35.9°, and 39.8° (Table 1, entry 2, 5, 6, 7, 9, 10, 12, and 13), the crystallite sizes of the Biofield Energy Treated sample were significantly increased from 9% to 67% compared with the control sample. The average crystallite size was overall increased in the Biofield Energy Treated magnesium gluconate by 6.13% compared to the control sample. Scientific literature reported that the changes in the XRD patterns, such as crystallite size and relative intensities, indicated the modification of the morphology of the crystal as well as the proof of polymorphic transition [47, 48]. As the crystal morphology of the Biofield Energy Treated sample was altered compared with the control sample, the Biofield Energy Treated sample might be a new polymorphic form of magnesium gluconate. The crystal pattern, size and even polymorphic form of a pharmaceutical play important roles in drug solubility, dissolution and bioavailability. It has been reported in the literature that the alteration in crystal morphology has significant impact on the *in vitro* dissolution rate, with potential for enhancing the bioavailability [43]. So, it can be concluded that the Biofield Energy Healing Treatment might be a very useful method for enhancing the bioavailability of magnesium gluconate.

3.2. Particle Size Distribution (PSD) Analysis

The particle size (d_{10}, d_{50}, and d_{90}) and surface area of both the control and Biofield Energy Treated samples were investigated and the results are presented in Table 2. The control magnesium gluconate displayed particle size value at d_{50} (38.51 μm) and d_{90} (182.41 μm). However, after the Biofield Energy Treatment, the magnesium gluconate showed particle size values as 39.57 μm and 189.20 μm for d_{50} and d_{90}, respectively. Thus, the Biofield Energy Treatment increased both the d_{50} (2.75%) and d_{90} (3.72%) values of the magnesium gluconate with respect to the control sample. On the other hand, the size of the particles at below 10% level (d_{10}) of the Biofield Energy Treated magnesium gluconate (6.05 μm) was decreased by 13.20% compared to the control sample (6.97 μm).

Table 2. *Particle size data (d_{10}, d_{50}, and d_{90}) and surface area of the control and Biofield Energy Treated magnesium gluconate.*

Test Item	d_{10} (μm)	d_{50} (μm)	d_{90} (μm)	Surface area (m²/g)
Control	6.97	38.51	182.41	0.359
Biofield Treated	6.05	39.57	189.20	0.384
Percent change* (%)	-13.20	2.75	3.72	6.964

*denotes the percentage change in the particle size data (d_{10}, d_{50}, and d_{90}) and surface area of the Biofield Energy Treated sample with respect to the control sample.

The surface area analysis revealed that the surface area of the Biofield Energy Treated magnesium gluconate (0.384 m²/g) was improved by 6.964% from the surface area of the control magnesium gluconate (0.359 m²/g) as shown in Table 2.

Poorly crystallized compounds possess more surface area and higher exchange capacities than well-crystallized compounds [49]. In addition, the variation of the crystal morphology in the Biofield Energy Treated sample, which was well-supported from PXRD data, may cause to alter the surface area of the Biofield Energy Treated magnesium gluconate in comparison with the control sample. It has been well established that the particle size, shape and surface area of pharmaceutical compounds have an important impact on solubility, dissolution and *in vivo* bioavailability, as well as in helping the design of new drug delivery systems [50, 51]. Reducing particle size and higher surface area would enhance the solubility of the solid particles and consequently, would increase the dissolution rate and bioavailability [52]. Thus, it is assumed that the Biofield Energy Treated magnesium gluconate might be dissolved and absorbed at a faster rate and may possibly have more bioavailability than normal magnesium gluconate.

3.3. Fourier Transform Infrared (FT-IR) Spectroscopy

The FT-IR spectra of both the control and Biofield Energy Treated samples (Figure 2), exhibited only one broad band of high intensity in the range from 3200 to 3600 cm⁻¹ with centroid at 3400 cm⁻¹. This peak was ascribed to the stretching vibrations of hydroxyl groups originating from the water present in magnesium gluconate. The bands of stretching vibrations of primary and secondary hydroxyl groups from the gluconate part of the compound appeared in this region. These bands were remained invisible due to the intensive broad band of water [53]. The absorption peaks for the deformation vibration of the hydroxyl groups in the plane δ (OH) and out-of-plane γ (OH) that indicate the presence of primary and secondary hydroxyl groups were observed at 1434 cm⁻¹ and 636 cm⁻¹ and 577 cm⁻¹, respectively in the spectra of both the control and the Biofield Energy Treated samples. The FT-IR spectrum of the control sample showed C-H stretching at 2932 cm⁻¹ and 1380 cm⁻¹, whereas these bands were observed at 2933 cm⁻¹ and 1380 cm⁻¹ in the Biofield Energy Treated magnesium gluconate. A very sharp and intensive band at 1606 cm⁻¹ for C=O stretching vibration of a carbonyl group of carboxylate anion was observed in the spectra of both the control and Biofield Energy Treated magnesium gluconate. The band of the C-O stretching vibrations of the primary alcohol group was perceived at 1056 cm⁻¹ in the spectra of both the control and Biofield Energy Treated magnesium gluconate. The absorption peaks at 1229 cm⁻¹ and 1142 cm⁻¹ due to the C-O stretching vibrations of the secondary alcohol groups were observed in the spectra of both the control and Biofield Energy Treated magnesium gluconate.
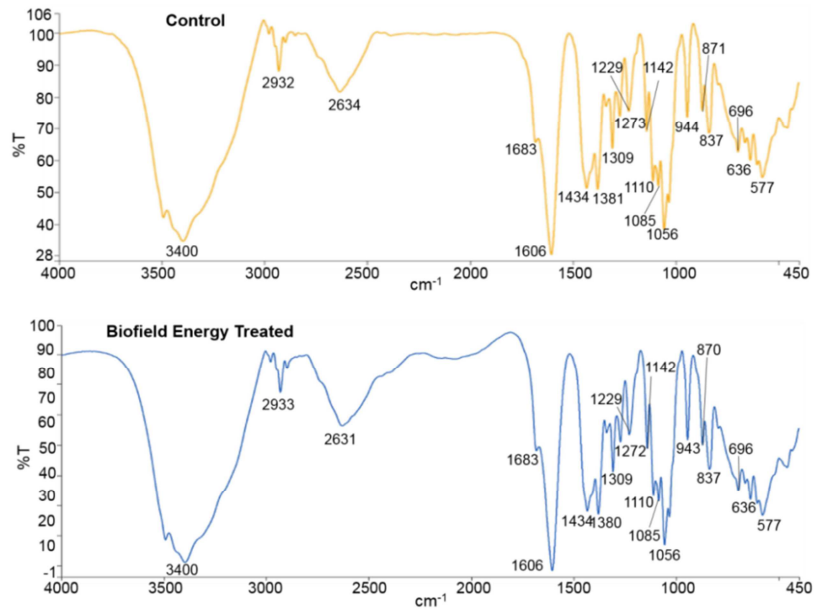
Figure 2. FT-IR spectra of the control and Biofield Energy Treated magnesium gluconate.

The FT-IR analysis indicated that there was no significant alteration of the characteristic peaks for the functional groups. Hence, it can be concluded that the structure of magnesium gluconate remained the same in both the Biofield Energy Treated and control samples.

3.4. Ultraviolet-Visible Spectroscopy (UV-Vis) Analysis

Literature reported that 0.1% aqueous solution of magnesium gluconate showed a maximum absorption peak (λ_{max}) at 194.7 nm [54]. The UV-vis spectra of both the control and Biofield Energy Treated samples (Figure 3) showed that the wavelength for the maximum absorbance (λ_{max}) of both the control and Biofield Energy Treated samples were at 198.1 nm and 197.9 nm, respectively with a minor shift of absorbance maxima from 2.2347 (control sample) to 2.2225 (the Biofield Energy Treated sample).
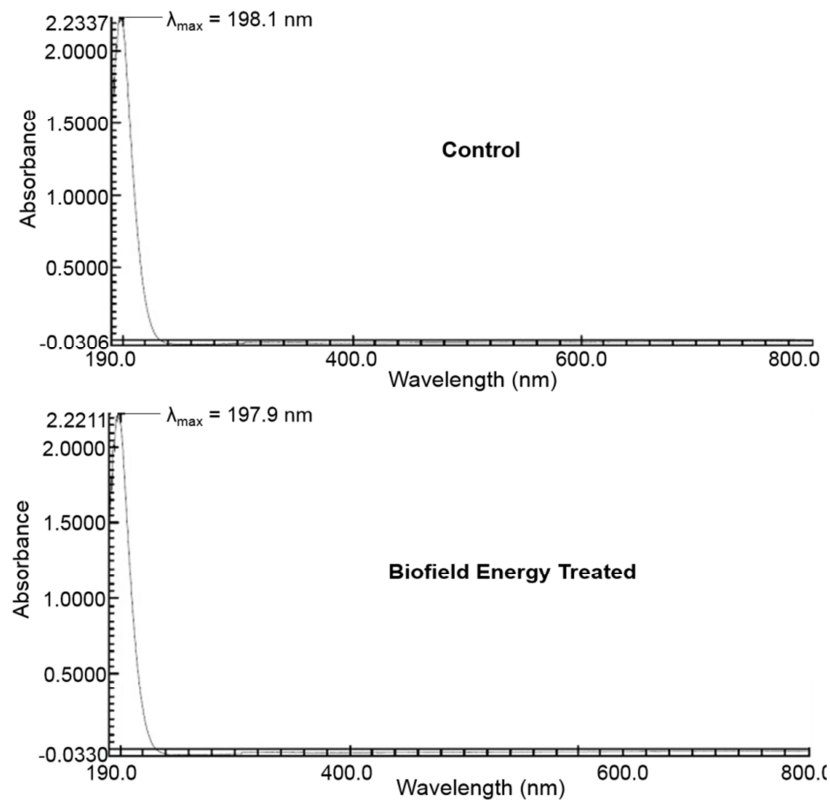

Figure 3. UV-Vis spectra of the control and Biofield Energy Treated magnesium gluconate.

The UV absorbance happens due to the different types of energy transitions from the singlet to the singlet excited state such as $\sigma \to \sigma^*$, $n \to \pi^*$, and $\pi \to \pi^*$. These types of electronic transitions are occurred when the difference in energy between the lowest unoccupied molecular orbital (LUMO) and the highest occupied molecular orbital (HOMO) is significantly higher than the activation energy of the compound [55]. As there was no significant alternation in the λ_{max} of the Biofield Energy Treated sample compared with the control, it is inferred that the structural configuration

or activation energy of the Biofield Energy Treated sample was not different from the control sample.

3.5. Thermal Gravimetric Analysis (TGA)/ Differential Thermogravimetric (DTG) Analysis

The TGA study of both the control and the Biofield Energy Treated samples (Figure 4) exhibited three thermal degradation steps and the data are presented in Table 3.

Table 3. Thermal degradation steps of the control and Biofield Energy Treated magnesium gluconate.

S. No.	Temperature (°C)		% Weight loss		% Change*
	Control	Treated	Control	Treated	
1st step of degradation	140.64	139.04	1.73	1.68	-2.89
2nd step of degradation	258.12	247.73	39.15	35.85	-8.43
3rd step of degradation	896.03	896.09	38.50	44.20	14.80
Total weight loss	-	-	79.38	81.73	2.96

*denotes the percentage change in the weight loss of the Biofield Energy Treated sample with respect to the control sample.

The weight loss of the Biofield Energy Treated sample at the first degradation step (1.68%) and second degradation step (35.85%) was reduced by 2.89% and 8.43%, respectively compared with the control sample (1st step = 1.73% and 2nd step = 39.15%). In contrast, the weight loss of

the Biofield Energy Treated magnesium gluconate at the third step of degradation (44.20%) was increased by 14.80% compared with the control sample (38.50%). The first degradation step was probably associated with the elimination of water of both the samples.
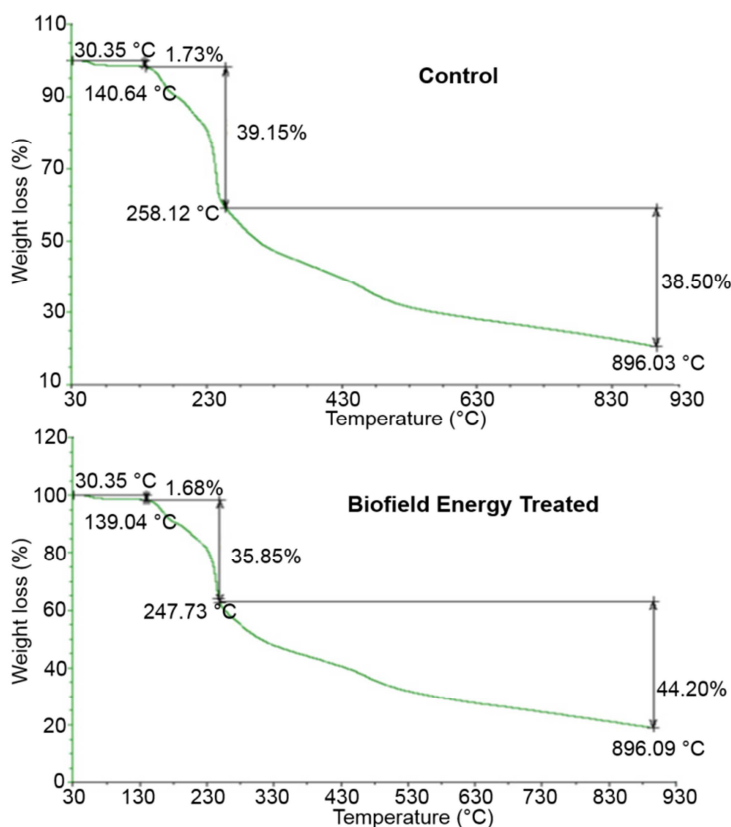

Figure 4. TGA thermograms of both the control and Biofield Energy Treated magnesium gluconate.

Overall, the total weight loss of the Biofield Energy Treated sample was slightly (2.96%) raised with respect to the control sample. The differential thermogravimetric (DTG) thermogram of both the control and Biofield Energy

Treated sample (Figure 5) exhibited that the control sample showed two major peaks at 164.95°C and 243.77°C along with two other minor peaks at 58.19°C and 203.49°C.
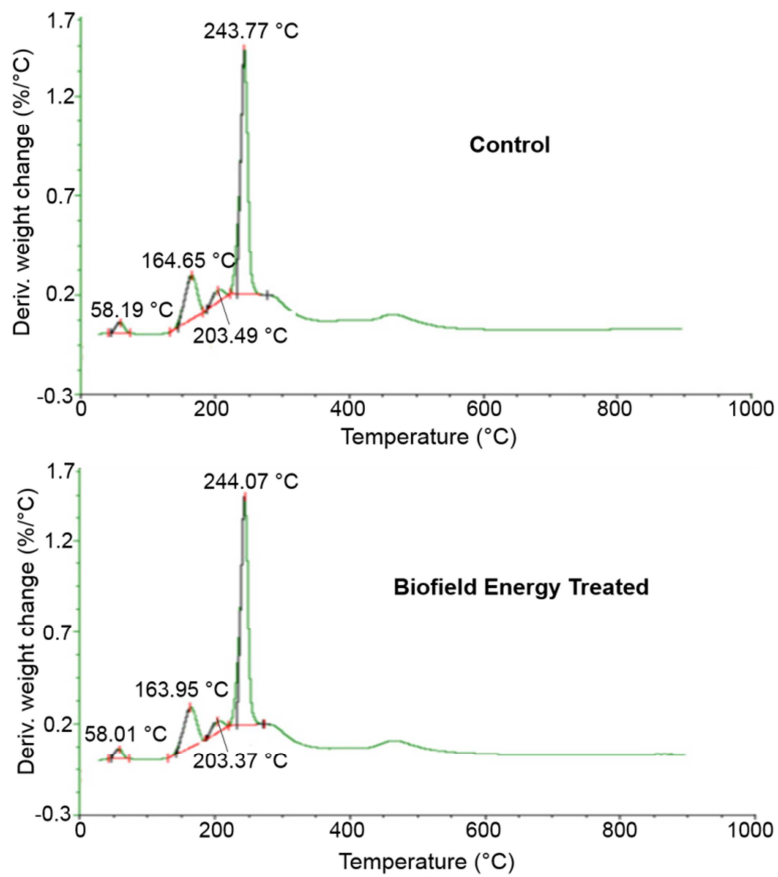
Figure 5. *DTG thermogram of the control and Biofield Energy Treated magnesium gluconate.*
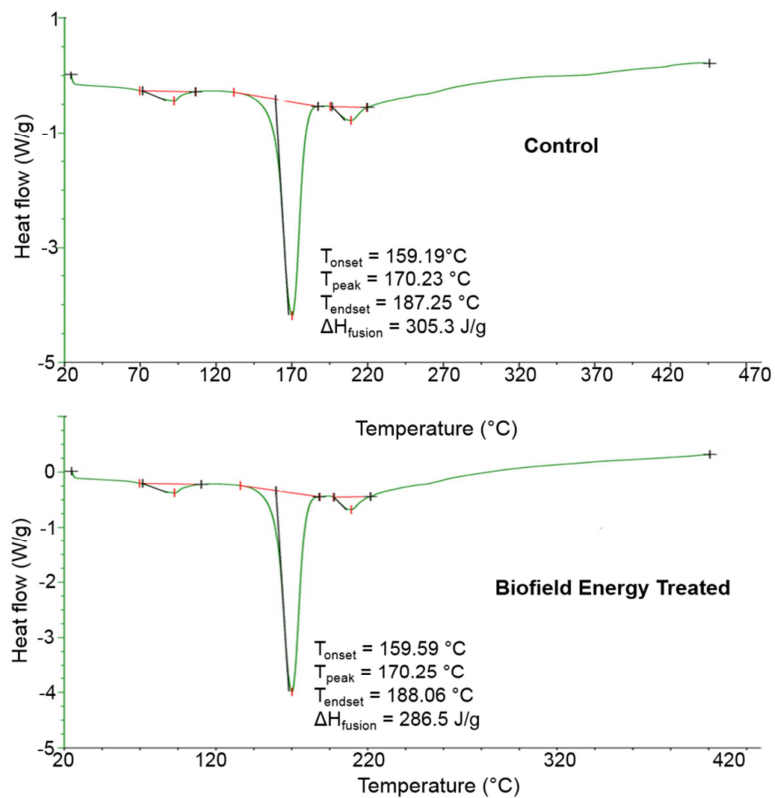

Figure 6. *DSC thermograms of the control and Biofield Energy Treated magnesium gluconate.*

In contrast, the major peaks in the Biofield Energy Treated sample were observed at 163.95°C and 244.07°C and the minor peaks were at 58.01°C and 203.37°C. So, the Biofield Energy Treated sample displayed a similar thermal decomposition pattern with the control sample. However, the analysis results indicated that there was very minor alteration in the thermal stability of the Biofield Energy Treated magnesium gluconate with respect to the control sample.

3.6. Differential Scanning Calorimetry (DSC) Analysis

The DSC thermograms of both the control and Biofield Energy Treated samples of magnesium gluconate are presented in Figure 6. The DSC thermogram of the control sample showed the presence of an endothermic sharp inflection at 170.23°C, which was due to the melting temperature of the sample. However, the Biofield Energy Treated magnesium gluconate displayed an endothermic peak at 170.25°C, which corresponded to the melting temperature of the Biofield Energy Treated sample. This suggested that there was no change in the melting temperature of the Biofield Energy Treated magnesium gluconate with respect to the control. The control and Biofield Energy Treated magnesium gluconate exhibited a latent heat of fusion of 305.3 J/g and 286.5 J/g, respectively. The result showed 6.15% decrease in the latent heat of fusion in the Biofield Energy Treated magnesium gluconate compared with the control sample (Table 4).

Table 4. *The latent heat of fusion (J/G) and melting point (°C) values of the control and Biofield Energy Treated magnesium gluconate.*

Sample	Latent heat of fusion (ΔH) J/g	Onset melting temperature (T_{onset}) °C	Peak melting temperature (T_{peak}) °C	Endset melting temperature (T_{endset}) °C
Control	305.3	159.19	170.23	187.25
Biofield Energy Treated	286.5	159.59	170.25	188.06
% Change[*]	-6.15	0.25	0.01	0.43

T_{onset}: Onset melting temperature, T_{peak}: Peak melting temperature, T_{endset}: Endset melting temperature, ΔH: Latent heat of fusion, [*]denotes the percentage change of the Biofield Energy Treated sample with respect to the control sample.

Literature demonstrated that decreased particle size reduced the latent heat of fusion [56]. According to the DSC data and the reported literature, it is hypothesized that the Biofield Energy Treated sample might be the enantiotropic form of the untreated magnesium gluconate. The Biofield Energy Treated sample, having a lower latent heat of fusion, might be a more stable and soluble polymorphic form at temperature below the transition point [57, 58].

4. Conclusions

The current analysis anticipated the remarkable impact of the Biofield Energy Healing (The Trivedi Effect[®]) on physicochemical, structural, thermal, and behavioral properties of magnesium gluconate. The PXRD analysis showed that the crystallite size of the Biofield Energy Treated magnesium gluconate was significantly changed in the range from - 33.33% to 66.65% with respect to the control sample. The average crystallite size was increased in the Biofield Energy Treated magnesium gluconate by 6.13% compared with the control sample. Overall, the PXRD analysis indicated the alteration of the crystal morphology in the Biofield Energy Treated sample compared with the control sample. Particle size analysis revealed that the particle size at d_{10} value of the Biofield Energy Treated sample was significantly reduced by 13.19% and the particle size at d_{50} and d_{90} values were increased by 2.75% and 3.72%, respectively compared with the control sample. The surface area analysis disclosed that the surface area of the Biofield Energy Treated sample was increased by 6.964% compared with the control sample. The DSC analysis showed 6.15% decrease in the latent heat of fusion in the Biofield Energy Treated magnesium gluconate compared to the control sample, while the melting point of the

control and treated samples were at 170.23°C and 170.25°C, respectively. A conclusive finding obtained from the PXRD, particle size, surface area and DSC analysis was that the Biofield Energy Treated magnesium gluconate could be a new polymorphic form of magnesium gluconate, which might have improved solubility, more bioavailability and long-term storage stability compared with the control sample. Thus, The Trivedi Effect[®] - Energy of Consciousness Healing Treatment, could be a useful approach in the design of better nutraceutical and/or pharmaceutical formulations that can offer significant therapeutic responses against various diseases such as diabetes mellitus, allergies and septic shock, stress-related disorders like sleep disorder, insomnia, anxiety, depression, Attention Deficit Disorder (ADD), Attention Deficit Hyperactive Disorder (ADHD), mental restlessness (mind chattering), brain frog, low libido, impotency, lack of motivation, mood swings, fear of the future, confusion, migraines, headaches, forgetfulness, overwhelm, loneliness, worthlessness, indecisiveness, frustration, irritability, chronic fatigue, obsessive/compulsive behavior and panic attacks; inflammatory diseases and immunological disorders like Lupus, Systemic Lupus Erythematosus, Hashimoto Thyroiditis, Type 1 Diabetes, Asthma, Chronic peptic ulcers, Tuberculosis, Hepatitis, Chronic active hepatitis, Celiac Disease (gluten-sensitive enteropathy), Addison Disease, Crohn's disease, Graves' Disease, Pernicious and Aplastic Anemia, Sjogren Syndrome, Irritable Bowel Syndrome (IBS), Multiple Sclerosis, Rheumatoid arthritis, Chronic periodontitis, Ulcerative colitis, Chronic sinusitis, Myasthenia Gravis, Atherosclerosis, Vasculitis, Dermatitis, Diverticulitis, Rheumatoid Arthritis, Reactive Arthritis, Alopecia Areata, Psoriasis, Scleroderma, Fibromyalgia, Chronic Fatigue Syndrome and Vitiligo, aging-related diseases like

cardiovascular disease, arthritis, cancer, Alzheimer's disease, dementia, cataracts, osteoporosis, diabetes, hypertension, glaucoma, hearing loss, Parkinson's Disease, Huntington's Disease, Prion Disease, Motor Neurone Disease, Spinocerebellar Ataxia, Spinal muscular atrophy, Amyotrophic lateral sclerosis, Friedreich's Ataxia and Lewy Body Disease; chronic infections and much more.

Abbreviations

DSC: Differential scanning calorimetry, DTG: Differential Thermogravimetric, FT-IR: Fourier transform infrared spectroscopy, FWHM: Full width half maximum, G: Crystallite size, HOMO: Highest energy occupied molecular orbital, LUMO: Lowest energy unoccupied molecular orbital, TGA: Thermal gravimetric analysis, T_{onset}: Onset melting temperature, T_{peak}: Peak melting temperature, T_{endset}: Endset melting temperature, ΔH: Latent heat of fusion, UV-vis: Ultraviolet-visible spectroscopy, PSD: Particle size distribution; PXRD: Powder X-ray diffraction.

Acknowledgements

References

[1] Swaminathan R (2003) Magnesium metabolism and its disorders. Clin Biochem Rev 24: 47-66.

[2] Ronconi L, Sadler PJ (2008) Applications of heteronuclear NMR spectroscopy in biological and medicinal inorganic chemistry. Coordn Chem Rev 252: 2239-2277.

[3] Trivedi MK, Tallapragada RM, Branton A, Trivedi D, Nayak G, Latiyal O, Jana S (2015) Potential impact of biofield treatment on atomic and physical characteristics of magnesium. Vitam Miner 3: 129.

[4] Guerrera MP, Volpe SL, Mao JJ (2009) Therapeutic uses of magnesium. Am Fam Physician 80: 157-162.

[5] Gums JG (2004) Magnesium in cardiovascular and other disorders. Am J Health Syst Pharm 61: 1569-1576.

[6] Purvis JR, Movahed A (1992) Magnesium disorders and cardiovascular diseases. Clin Cardiol 5: 556-568.

[7] Sales CH, Pedrosa Lde F (2006) Magnesium and diabetes mellitus: Their relation. Clin Nutr 25: 554-562.

[8] Nageris BI, Ulanovski D, Attias J (2004) Magnesium treatment for sudden hearing loss. Ann Otol Rhinol Laryngol 113: 672-675.

[9] Lysakowski C, Dumont L, Czarnetzki C, Tramer MR (2007) Magnesium as an adjuvant to postoperative analgesia: A systematic review of randomized trials. Anesth Analg 104: 1532-1539.

[10] Murphy JD, Paskaradevan J, Eisler LL, Ouanes JP, Tomas VA, Freck EA, Wu CL (2013) Analgesic efficacy of continuous intravenous magnesium infusion as an adjuvant to morphine for postoperative analgesia: A systematic review and meta-analysis. Middle East J Anaesthesiol 22: 11-20.

[11] Ramachandran S, Fontanille P, Pandey A, Larroche C (2006) Gluconic acid: Properties, applications and microbial production. Food Technol Biotechnol 44: 185-195.

[12] Fleming TE, Mansmann Jr HC (1999) Methods and compositions for the prevention and treatment of diabetes mellitus. United States Patent 5871769, 1-10.

[13] Fleming TE, Mansmann Jr HC (1999) Methods and compositions for the prevention and treatment of immunological disorders, inflammatory diseases and infections. United States Patent 5939394, 1-11.

[14] Weglicki WB (2000) Intravenous magnesium gluconate for treatment of conditions caused by excessive oxidative stress due to free radical distribution. United States Patent 6100297, 1-6.

[15] Martin RW, Martin JN Jr, Pryor JA, Gaddy DK, Wiser WL, Morrison JC (1988) Comparison of oral ritodrine and magnesium gluconate for ambulatory tocolysis. Am J Obstet Gynecol 158: 1440-1445.

[16] Jahnen-Dechent W, Ketteler M (2012) Magnesium basics. Clin Kidney J 5: i3-i14.

[17] Fine KD, Santa Ana CA, Porter JL, Fordtran JS (1991) Intestinal absorption of magnesium from food and supplements. J Clin Invest 88: 396-402.

[18] Coudray C, Rambeau M, Feillet-Coudray C, Gueux E, Tressol JC, Mazur A, Rayssiguier Y (2005) Study of magnesium bioavailability from ten organic and inorganic Mg salts in Mg-depleted rats using a stable isotope approach. Magnes Res 18: 215-223.

[19] Stenger VJ (1999) Bioenergetic fields. Sci Rev Alternative Med 3.

[20] Rogers, M (1989) "Nursing: A Science of Unitary Human Beings." In J. P. Riehl-Sisca (ed.) Conceptual Models for Nursing Practice. 3rd edition. Norwalk: Appleton & Lange.

[21] Warber SL, Cornelio D, Straughn, J, Kile G (2004) Biofield energy healing from the inside. J Altern Complement Med 10: 1107-1113.

[22] Koithan M (2009) Introducing complementary and alternative therapies. J Nurse Pract 5: 18-20.

[23] Trivedi MK, Patil S, Shettigar H, Singh R, Jana S (2015) An impact of biofield treatment on spectroscopic characterization of pharmaceutical compounds. Mod Chem Appl 3: 159.

[24] Trivedi MK, Branton A, Trivedi D, Nayak G, Bairwa K, Jana S (2015) Spectroscopic characterization of disulfiram and nicotinic acid after biofield treatment. J Anal Bioanal Tech 6: 265.

[25] Trivedi MK, Branton A, Trivedi D, Nayak G, Singh R, Jana S (2015) Physicochemical and spectroscopic characterization of biofield treated butylated hydroxytoluene. J Food Ind Microbiol 1: 101.

[26] Trivedi MK, Tallapragada RM, Branton A, Trivedi D, Nayak G, Mishra RK, Jana S (2015) Biofield treatment: A potential strategy for modification of physical and thermal properties of gluten hydrolysate and ipomoea macroelements. J Nutr Food Sci 5: 414.

[27]   Trivedi MK, Tallapragada RM, Branton A, Trivedi D, Nayak G, Latiyal O, Jana S (2015) Physical, atomic and thermal properties of biofield treated lithium powder. J Adv Chem Eng 5: 136.

[28]   Trivedi MK, Branton A, Trivedi D, Nayak G, Bairwa K, Jana S (2015) Fourier transform infrared and ultraviolet-visible spectroscopic characterization of ammonium acetate and ammonium chloride: An impact of biofield treatment. Mod Chem appl 3: 163.

[29]   Trivedi MK, Branton A, Trivedi D, Nayak G, Latiyal O, Jana S (2015) Evaluation of biofield treatment on atomic and thermal properties of ethanol. Organic Chem Curr Res 4: 145.

[30]   Trivedi MK, Branton A, Trivedi D, Nayak G, Singh R, Jana S (2016) Characterization of physical, thermal and spectroscopic properties of biofield treated ortho-toluic acid. J O Heterocyclics 106: 21-28.

[31]   Trivedi MK, Tallapragada RM, Branton A, Trivedi D, Latiyal O, Jana S (2015) Influence of biofield treatment on physical and structural characteristics of barium oxide and zinc sulfide. J Laser Opt Photonics 2: 122.

[32]   Trivedi MK, Nayak G, Patil S, Tallapragada RM, Latiyal O (2015) Evaluation of biofield treatment on physical, atomic and structural characteristics of manganese (II, III) oxide. J Material Sci Eng 4: 177.

[33]   Trivedi MK, Nayak G, Patil S, Tallapragada RM, Latiyal O (2015) Studies of the atomic and crystalline characteristics of ceramic oxide nano powders after bio field treatment. Ind Eng Manage 4: 161.

[34]   Trivedi MK, Branton A, Trivedi D, Nayak G, Bairwa K, Jana S (2015) Physical, thermal, and spectroscopic characterization of biofield energy treated murashige and skoog plant cell culture media. Cell Biology 3: 50-57.

[35]   Nayak G, Altekar N (2015) Effect of a biofield treatment on plant growth and adaptation. J Environ Health Sci 1: 1-9.

[36]   Trivedi MK, Branton A, Trivedi D, Nayak G, Mondal SC, Jana S (2015) Impact of biofield energy treatment on soil fertility. Earth Sciences 4: 275-279.

[37]   Trivedi MK, Branton A, Trivedi D, Nayak G, Mondal SC, Jana S (2015) Antimicrobial sensitivity, biochemical characteristics and biotyping of *Staphylococcus saprophyticus*: An impact of biofield energy treatment. J Women's Health Care 4: 271.

[38]   Trivedi MK, Branton A, Trivedi D, Nayak G, Gangwar M, Jana S (2015) Use of energy healing medicine against *Escherichia coli* for antimicrobial susceptibility, biochemical reaction and biotyping. American Journal of Bioscience and Bioengineering. 3: 99-105.

[39]   Trivedi MK, Branton A, Trivedi D, Shettigar H, Nayak G, Mondal SC, Jana S (2015) Phenotyping and genotyping characterization of *Proteus vulgaris* after biofield treatment. International Journal of Genetics and Genomics 3: 66-73.

[40]   Trivedi MK, Patil S, Shettigar H, Gangwar M, Jana S (2015) *In vitro* evaluation of biofield treatment on cancer biomarkers involved in endometrial and prostate cancer cell lines. J Cancer Sci Ther 7: 253-257.

[41]   Ranade VV, Somberg JC (2001) Bioavailability and pharmacokinetics of magnesium after administration of magnesium salts to humans. Am J Ther 8: 345-357.

[42]   Chereson R (2009) Bioavailability, bioequivalence, and drug selection. In: Makoid CM, Vuchetich PJ, Banakar UV (eds) Basic pharmacokinetics (1st Edn) Pharmaceutical Press, London.

[43]   Blagden N, de Matas M, Gavan PT, York P (2007) Crystal engineering of active pharmaceutical ingredients to improve solubility and dissolution rates. Adv Drug Deliv Rev 59: 617-630.

[44]   Trivedi MK, Mohan TRR (2016) Biofield energy signals, energy transmission and neutrinos. American Journal of Modern Physics 5: 172-176.

[45]   Alexander L, Klug HP (1950) Determination of crystallite size with the X-Ray Spectrometer. J App Phys 21: 137.

[46]   Langford JI, Wilson AJC (1978) Scherrer after sixty years: A survey and some new results in the determination of crystallite size. J Appl Cryst 11: 102-113.

[47]   Inoue M, Hirasawa I (2013) The relationship between crystal morphology and XRD peak intensity on $CaSO_4$. $2H_2O$. J Crystal Growth 380: 169-175.

[48]   Raza K, Kumar P, Ratan S, Malik R, Arora S (2014) Polymorphism: The phenomenon affecting the performance of drugs. SOJ Pharm Pharm Sci 1: 10.

[49]   Murray HH, Lyons SC (1960) Further correlation of kaolinite crystallinity with chemical and physical properties. Clays Clay Miner 8: 11-17.

[50]   Sun J, Wang F, Sui Y, She Z, Zhai W, Wang C, Deng Y (2012) Effect of particle size on solubility, dissolution rate, and oral bioavailability: Evaluation using coenzyme Q_{10} as naked nanocrystals. Int J Nanomed 7: 5733-5744.

[51]   Khadka P, Ro J, Kim H, Kim I, Kim JT, Kim H, Cho JM, Yun G, Lee J (2014) Pharmaceutical particle technologies: An approach to improve drug solubility, dissolution and bioavailability. Asian J Pharm Sci 9: 304-316.

[52]   Buckton G, Beezer AE (1992) The relationship between particle size and solubility. Int J Pharmaceutics 82: R7-R10.

[53]   Nikolic VD, Illic DP, Nikolic LB, Stanojevic LP, Cakic MD, Tacic AD, Ilic-Stojanovic SS (2014) The synthesis and characterization of iron (II) gluconate. Advanced technologies 3: 16-24.

[54]   Ji L, Yin W, Fu-Jia M (2004) Confirmation of the chemical structure of magnesium gluconate. Pharmaceutical Care and Research 4: 272-273.

[55]   Hesse M, Meier H, Zeeh B (1997) Spectroscopic methods in organic chemistry, Georg Thieme Verlag Stuttgart, New York.

[56]   Zhang M, Efremov MY, Schiettekatte F, Olson EA, Kwan AT, Lai SL, Wisleder T, Greene JE, Allen LH (2000) Size-dependent melting point depression of nanostructures: Nanocalorimetric measurements. Phys Rev B 62: 10548.

[57]   Lee EH (2014) A practical guide to pharmaceutical polymorph screening & selection. Asian J Pharm Sci 9: 163-175.

[58]   Brittain HG (2009) Polymorphism in pharmaceutical solids in Drugs and Pharmaceutical Sciences, volume 192, 2nd Edn, Informa Healthcare USA, Inc., New York.